Stimuli-Responsive Polymer Nanocomposites Inspired by the Sea Cucumber Dermis

Jeffrey R. Capadona, *et al.*

Science **319**, 1370 (2008);
DOI: 10.1126/science.1153307

processes in the fiber, in particular stimulated Raman scattering (*20*), limit the optical shock. Assuming that the steepness at the shock front is comparable to twice the frequency of the pulse carrier, 8×10^{14} Hz, the Hawking temperature (Eq. 8) reaches 10^3 K, which is many orders of magnitude higher than that in condensed-matter analogs of the event horizon (*10*–*12*, *18*).

Our scheme thus solves two problems at once in a natural way: how to let an effective medium move at superluminal speed, and how to generate a steep velocity profile at the horizon. Here the various aspects of the physics of artificial black holes conspire together, in contrast to most other proposals (*1*–*4*, *10*–*16*).

References and Notes

1. *Artificial Black Holes*, M. Novello, M. Visser, G. E. Volovik, Eds. (World Scientific, Singapore, 2002).
2. G. E. Volovik, *The Universe in a Helium Droplet* (Clarendon Press, Oxford, 2003).
3. W. G. Unruh, R. Schützhold, *Quantum Analogues: From Phase Transitions to Black Holes and Cosmology* (Springer, Berlin, 2007).
4. W. G. Unruh, *Phys. Rev. Lett.* **46**, 1351 (1981).
5. T. Jacobson, *Prog. Theor. Phys.* **136** (suppl.), 1 (1999).
6. G. Rousseaux, C. Mathis, P. Maïssa, T. G. Philbin, U. Leonhardt, http://arxiv.org/abs/0711.4767.
7. S. M. Hawking, *Nature* **248**, 30 (1974).
8. N. D. Birrell, P. C. W. Davies, *Quantum Fields in Curved Space* (Cambridge Univ. Press, Cambridge, 1984).
9. R. Brout, S. Massar, R. Parentani, Ph. Spindel, *Phys. Rep.* **260**, 329 (1995).
10. L. J. Garay, J. R. Anglin, J. I. Cirac, P. Zoller, *Phys. Rev. Lett.* **85**, 4643 (2000).
11. S. Giovanazzi, C. Farrell, T. Kiss, U. Leonhardt, *Phys. Rev. A* **70**, 063602 (2004).
12. S. Giovanazzi, *Phys. Rev. Lett.* **94**, 061302 (2005).
13. R. Schützhold, W. G. Unruh, *Phys. Rev. D* **66**, 044019 (2002).
14. G. E. Volovik, *J. Exp. Theor. Phys. Lett.* **76**, 240 (2002).
15. U. Leonhardt, P. Piwnicki, *Phys. Rev. Lett.* **84**, 822 (2000).
16. U. Leonhardt, *Nature* **415**, 406 (2002).
17. P. W. Milonni, *Fast Light, Slow Light and Left Handed Light* (Institute of Physics, Bristol, UK, 2004).
18. T. A. Jacobson, G. E. Volovik, *Phys. Rev. D* **58**, 064021 (1998).
19. R. Schützhold, W. G. Unruh, *Phys. Rev. Lett.* **95**, 031301 (2005).
20. G. Agrawal, *Nonlinear Fiber Optics* (Academic Press, San Diego, CA, 2001).
21. W. H. Reeves *et al.*, *Nature* **424**, 511 (2003).
22. P. Russell, *Science* **299**, 358 (2003).
23. G. t'Hooft. *Nucl. Phys. B* **256**, 727 (1985).
24. T. Jacobson, *Phys. Rev. D* **44**, 1731 (1991).
25. See the supporting material on *Science* Online.
26. U. Leonhardt, *Rep. Prog. Phys.* **66**, 1207 (2003).
27. *Few-Cycle Laser Pulse Generation and Its Applications*, F. X. Kärtner, Ed. (Springer, Berlin, 2004).
28. T. Brabec, F. Krausz, *Rev. Mod. Phys.* **72**, 545 (2000).

29. We are indebted to G. Agrawal, M. Dunn, T. Hänsch, A. Miller, R. Parentani, and W. Sibbett for discussions and technical support. We thank A. Podlipensky and P. Russell for measuring the dispersion of our fiber. Our work was supported by the Leverhulme Trust, Engineering and Physical Sciences Research Council, Continuous Variable Quantum Information with Atoms and Light, the Ultrafast Photonics Facility at St Andrews, and Leonhardt Group Aue.

Supporting Online Material

www.sciencemag.org/cgi/content/full/319/5868/1367/DC1
SOM Text
Figs. S1 to S13
Table S1
References and Notes

30 November 2007; accepted 24 January 2008
10.1126/science.1153625

Stimuli-Responsive Polymer Nanocomposites Inspired by the Sea Cucumber Dermis

Jeffrey R. Capadona,[1,2,3] Kadhiravan Shanmuganathan,[1] Dustin J. Tyler,[2,3] Stuart J. Rowan,[1,2,3,4]* Christoph Weder[1,2,4]*

Sea cucumbers, like other echinoderms, have the ability to rapidly and reversibly alter the stiffness of their inner dermis. It has been proposed that the modulus of this tissue is controlled by regulating the interactions among collagen fibrils, which reinforce a low-modulus matrix. We report on a family of polymer nanocomposites, which mimic this architecture and display similar chemoresponsive mechanic adaptability. Materials based on a rubbery host polymer and rigid cellulose nanofibers exhibit a reversible reduction by a factor of 40 of the tensile modulus, for example, from 800 to 20 megapascals (MPa), upon exposure to a chemical regulator that mediates nanofiber interactions. Using a host polymer with a thermal transition in the regime of interest, we demonstrated even larger modulus changes (4200 to 1.6 MPa) upon exposure to emulated physiological conditions.

Many echinoderms share the ability to rapidly and reversibly alter the stiffness of their connective tissue (*1*). In the case of sea cucumbers (Fig. 1, A and B), this morphing occurs within seconds and creates considerable survival advantages (*1*, *2*). A series of recent studies on the dermis of these invertebrates has provided evidence that this defense mechanism is enabled by a nanocomposite structure in which rigid, high-aspect ratio collagen fibrils reinforce a viscoelastic matrix of fibrillin microfibrils (*2*–*4*). The stiffness of the tissue is regulated by controlling the stress transfer between adjacent collagen fibrils through transiently established interactions (*5*, *6*). These interactions are modulated by soluble macromolecules that are secreted locally by neurally controlled effector cells. The dermis of the *Cucumaria frondosa* and other sea cucumber species represents a compelling model of a chemoresponsive material in which a modulus contrast by a factor of 10 (~5 to ~50 MPa) is possible (*7*). Intrigued by this capability and with the goal of creating new dynamic materials for biomedical applications, we set out to investigate whether nanocomposites can be created that exhibit similar architecture and properties. The control of nanofiber interactions exploited here in solid polymer materials is similar to that observed in aqueous dispersions of poly(acrylic acid)-coated carbon nanotubes (*8*) or cellulose nanofibers (*9*), which have been shown to exhibit large viscosity changes upon variation of pH. The materials further complement other polymeric systems with morphing mechanical behavior—for example, cross-linked polymers that change cross-link density upon a change in pH or ionic concentration (*10*, *11*).

The first series of nanocomposites studied is based on a rubbery ethylene oxide–epichlorohydrin 1:1 copolymer (EO-EPI) (Fig. 1C) into which a rigid cellulose nanofiber network was incorporated (Fig. 1, C and D). The EO-EPI matrix displays a low modulus and can accommodate the uptake of several chemical stimuli. Cellulose nanofibers, isolated for this study from the mantles of sessile sea creatures known as tunicates (*12*), were used as the reinforcing component. These "whiskers" exhibit high stiffness (tensile modulus ~143 GPa) (*13*) and dimensions at the nanometer scale (26 nm × 2.2 μm) (fig. S1). Similar nanofibers can be obtained from a range of renewable biosources, including wood and cotton. Whiskers from tunicates were used here because their aspect ratio is higher than that of cellulose from other sources, which is advantageous for the formation of percolating architectures. Because of the high density of strongly interacting surface hydroxyl groups, cellulose whiskers have a strong tendency for aggregation (*9*, *14*). The whisker-whisker interactions can be moderated by the introduction of sulfate surface groups (Fig. 1C), which promote dispersibility in select hydrogen-bond–forming solvents (*14*, *15*). This balance of attractive and repulsive interactions is the key for the fabrication of cellulose-whisker nanocomposites.

[1]Department of Macromolecular Science and Engineering, Case Western Reserve University, Cleveland, OH 44106, USA. [2]Rehabilitation Research and Development, Louis Stokes Cleveland DVA Medical Center, 10701 East Boulevard, Cleveland, OH 44106, USA. [3]Department of Biomedical Engineering, Case Western Reserve University, Cleveland, OH 44106, USA. [4]Department of Chemistry, Case Western Reserve University, 10900 Euclid Avenue, Cleveland, OH 44106, USA.

*To whom correspondence should be addressed. E-mail: christoph.weder@case.edu (C.W.); stuart.rowan@case.edu (S.J.R.)

Good dispersion is achieved during processing when whisker self-interactions are "switched off" by competitive binding with a hydrogen-bond–forming solvent (Fig. 1D) (*14*, *15*). Upon evaporation of the solvent, the interactions among the whiskers are "switched on," and they assemble into a percolating network. This architecture and strong interactions among the whiskers maximize stress transfer and therewith the overall modulus of the nanocomposite (*13*, *15*, *16*). Similar to the sea cucumber dermis, it should be possible to dynamically alter the modulus of the nanocomposites through the addition or removal of a chemical regulator that, in this case, would alter the extent of hydrogen bonding of the whiskers.

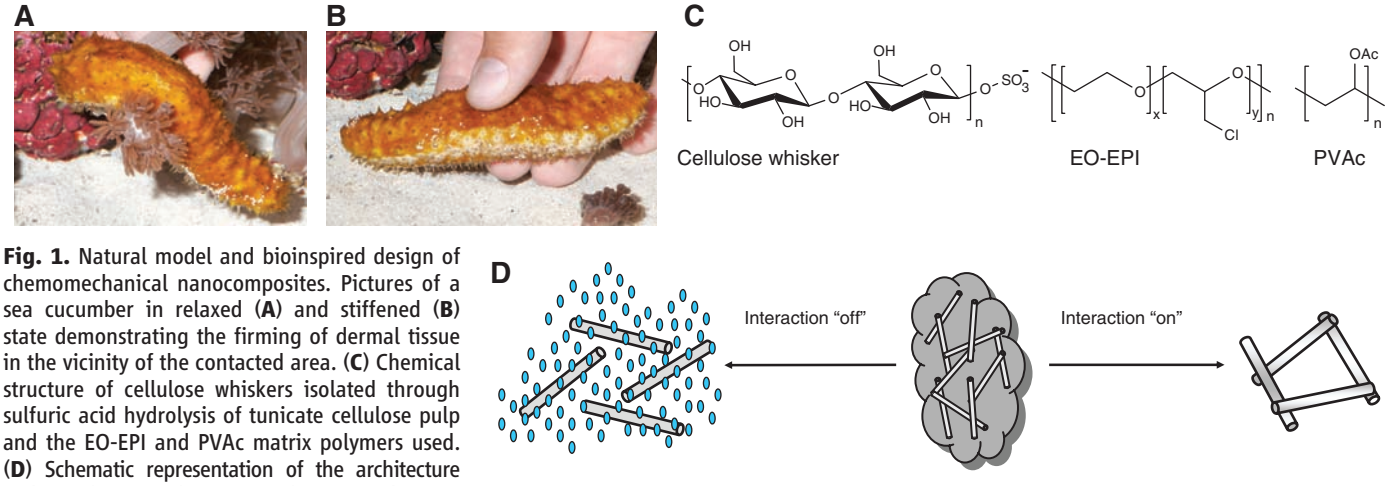

Fig. 1. Natural model and bioinspired design of chemomechanical nanocomposites. Pictures of a sea cucumber in relaxed (**A**) and stiffened (**B**) state demonstrating the firming of dermal tissue in the vicinity of the contacted area. (**C**) Chemical structure of cellulose whiskers isolated through sulfuric acid hydrolysis of tunicate cellulose pulp and the EO-EPI and PVAc matrix polymers used. (**D**) Schematic representation of the architecture and switching mechanism in the artificial nanocomposites with dynamic mechanical properties. In the "on" state, strong hydrogen bonds between rigid, percolating nanofibers maximize stress transfer and therewith the overall modulus of the nanocomposite. The interactions are switched "off" by the introduction of a chemical regulator that allows for competitive hydrogen bonding.

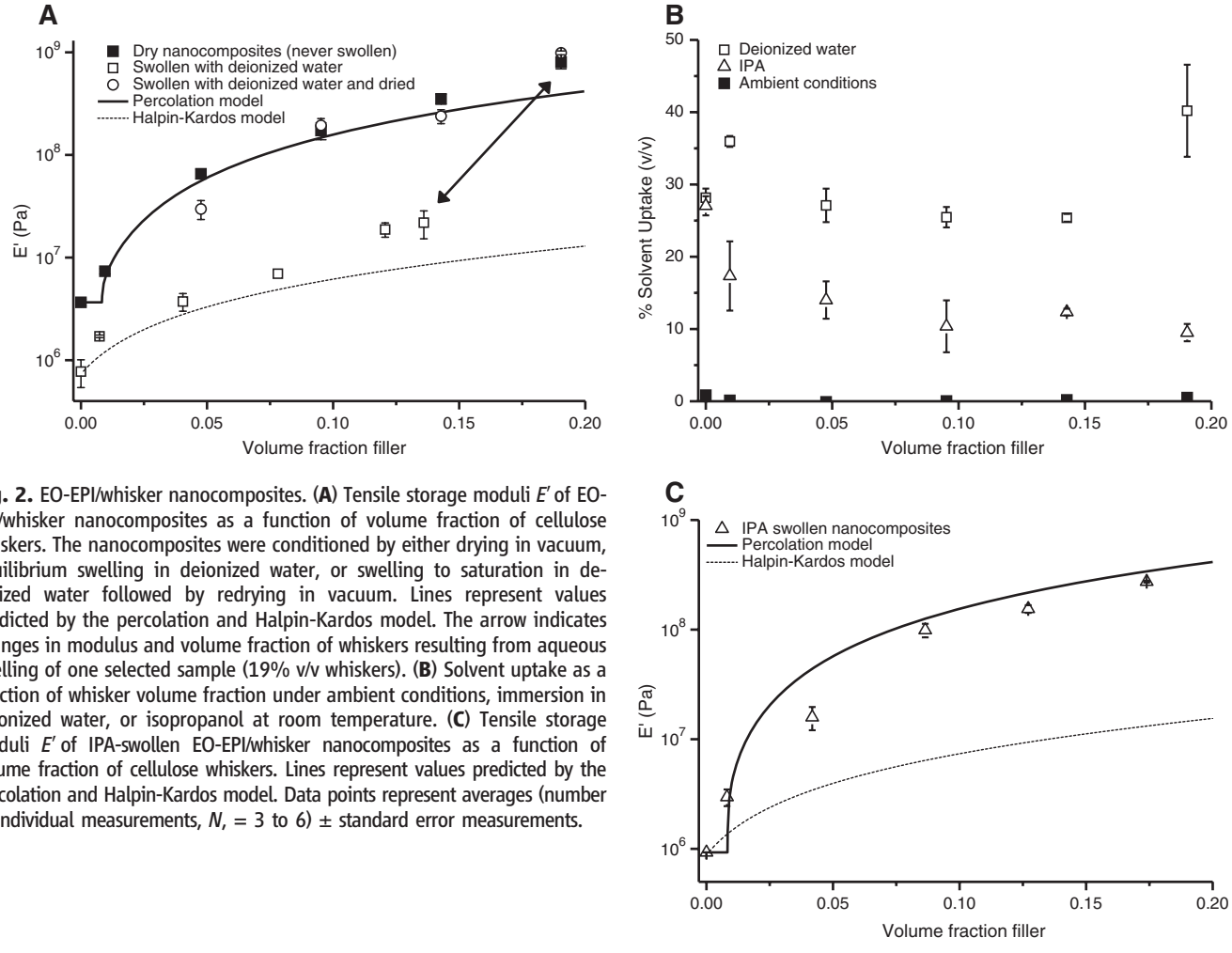

Fig. 2. EO-EPI/whisker nanocomposites. (**A**) Tensile storage moduli *E*′ of EO-EPI/whisker nanocomposites as a function of volume fraction of cellulose whiskers. The nanocomposites were conditioned by either drying in vacuum, equilibrium swelling in deionized water, or swelling to saturation in deionized water followed by redrying in vacuum. Lines represent values predicted by the percolation and Halpin-Kardos model. The arrow indicates changes in modulus and volume fraction of whiskers resulting from aqueous swelling of one selected sample (19% v/v whiskers). (**B**) Solvent uptake as a function of whisker volume fraction under ambient conditions, immersion in deionized water, or isopropanol at room temperature. (**C**) Tensile storage moduli *E*′ of IPA-swollen EO-EPI/whisker nanocomposites as a function of volume fraction of cellulose whiskers. Lines represent values predicted by the percolation and Halpin-Kardos model. Data points represent averages (number of individual measurements, *N*, = 3 to 6) ± standard error measurements.

EO-EPI/whisker nanocomposites were produced by solution casting from dimethylformamide (DMF), as previously reported (*16*), and the whisker content was varied between 0 and 19% v/v. The thermomechanical properties of these materials were established by dynamic mechanical analyses (DMA) and tensile tests. DMA temperature sweeps (figs. S2 and S3) display a glass transition temperature (T_g) around –37°C (maximum of loss tangent, tan δ), which is independent of the whisker content and matches the T_g of the neat EO-EPI matrix (fig. S2). The intensity of tan δ decreases more than proportionally with the whisker concentration (fig. S2), which is indicative of attractive polymer-whisker interactions. Figure 2A shows the tensile storage moduli (E') of dry EO-EPI/whisker nanocomposites extracted from the DMA traces for a temperature of 25°C, that is, in the rubbery regime far above T_g. E' increased with the whisker content from ~3.7 MPa (neat polymer) to ~800 MPa (19% v/v whiskers). The observed reinforcement suggests the formation of a percolating nanofiber network in which stress transfer is facilitated by hydrogen-bonding between the whiskers. This hypothesis is supported by calculations obtained using a percolation model (*16*). Within the framework of the model, the tensile storage modulus of the nanocomposites (E') can be expressed as (*17*, *18*)

$$E' = \frac{(1 - 2\psi + \psi X_r)E'_s E'_r + (1 - X_r)\psi E'^2_r}{(1 - X_r)E'_r + (X_r - \psi)E'_s} \quad (1)$$

with

$$\psi = X_r\left(\frac{X_r - X_c}{1 - X_c}\right)^{0.4} \quad (2)$$

where E'_s and E'_r are the experimentally determined tensile storage moduli of the neat EO-EPI (3.7 MPa) and a neat tunicate whisker film (4.0 GPa), respectively; ψ is the volume fraction of whiskers that participate in the load transfer; X_r is the volume fraction of whiskers; and X_c is the critical whisker percolation volume fraction calculated by $0.7/A$. A is the aspect ratio of the whiskers and has a value of 84 as determined by analysis of transmission electron microscopy (TEM) images (fig. S1). Figure 2A shows that the experimentally determined E' values of dry EO-EPI/whisker nanocomposites agree with values obtained from Eq. 1. By contrast, the data deviate strongly from the Halpin-Kardos model (fig. S4). This behavior is indicative for the formation of a percolating network of strongly interacting cellulose whiskers within the EO-EPI matrix (*15*, *16*). This architecture is confirmed by atomic force microscopy (AFM) (Fig. 3A) and scanning electron microscopy (SEM) (Fig. 3B) images, which both show that the cellulose whiskers form a percolating network within the EO-EPI matrix. Stress strain curves (fig. S5) reveal that the formation of a percolating network of cellulose whiskers within the EO-EPI matrix not only affects E' but also has a considerable influence on the maximum tensile strength (σ), which increased from 0.27 ± 0.04 (neat EO-EPI, stress at break) to 1.71 ± 0.23 MPa (14.3% v/v whiskers, stress at yield), whereas the elongation at break was reduced from 360 ± 20 to 6.7 ± 0.8% (table S1).

In view of the outstanding dispersibility of sulfate-modified cellulose whiskers in water (*15*), we elected to explore whether water could act as a chemical regulator for the whisker-whisker interactions in the EO-EPI/whisker nanocomposites. The atmospheric water uptake of the materials is negligible under ambient conditions, that is, if not placed in an aqueous medium (Fig. 2B). Dry EO-EPI/whisker nanocomposites were immersed in deionized water for 48 hours to achieve equilibrium swelling (Fig. 2B). Under these conditions, all compositions investigated exhibit modest aqueous swelling (~30% v/v), indicating that in the case of these compositions the water uptake is mainly governed by the matrix polymer with only minor variations due to whisker content. The tensile storage moduli for water-swollen EO-EPI/whisker nanocomposites were measured by DMA at 25°C in de-ionized water. A pronounced reduction of E' compared with the dry nanocomposites can be observed (Fig. 2A). The greatest mechanical contrast is seen in the case of the nanocomposite with the highest whisker content (nominally 19% v/v) (*19*), where E' was reduced from ~800 to 20 MPa upon equilibrium swelling. At the same time, swelling with water leads to a significant decrease of the tensile strength (1.71 ± 0.23 to 0.37 ± 0.11 MPa for a 14.3% v/v whisker nanocomposite) (fig. S5 and table S1) and an increase of the elongation at break (6.7 ± 0.8 to 17.8 ± 0.39%). Control experiments with the neat EO/EPI (fig. S5 and table S1) show minimal changes in tensile strength upon deionized water swelling.

One argument that could be made against the interpretation that the observed changes in modulus, elongation at break, and tensile strength are the result of switching off the nanofiber-nanofiber interactions is that simple swelling of the matrix alone could lead to a plasticizing effect; however, careful analysis of our data shows that this is not the case. DMA traces (fig. S2) indicate that the EO-EPI/whisker nanocomposites do not undergo any phase transition that would lead to a drop in modulus, such as cross-linked polymer hydrogels and hygroscopic polymers, which can display a decrease of the glass transition temperature upon water uptake (*20*). Although E'_s of the neat EO-EPI is reduced from 3.7 to 0.8 MPa upon equilibrium swelling with water (Fig. 2A), analysis in the context of the percolation model (Eqs. 1 and 2 and fig. S7) shows that a reduction of E'_s alone cannot account for a significant reduction of E'. Figure 2A also reveals that even after correcting X_r for water uptake, the percolation model no longer adequately describes E' of the water-swollen nanocomposites. By contrast, the moduli now are in much closer agreement with the Halpin-Kardos model (*21*), which has successfully been used to describe the modulus of nanocomposites in which the filler is homogeneously dispersed in a polymer matrix and does not display pronounced filler-filler interactions (*22*). The model assumes that the materials are equivalent to many layers of unidirectional plies oriented in alternating directions (–45°, 0°, 45°, and 90°), and the properties of the unidirectional reference ply are predicted by the Halpin-Tsaï equations where the tensile storage modulus in the longitudinal (E'_L) and transverse (E'_T) directions are given by (*22*, *23*)

$$E'_L = E'_s[1 + 2(A)\eta_L\phi_r]/(1 - \eta_L\phi_r) \quad (3)$$

and

$$E'_T = E'_s[1 + 2\eta_T\phi_r]/(1 - \eta_T\phi_r) \quad (4)$$

Thus, all data indicate that the stiffness reduction achieved in the EO-EPI/whisker nanocomposites is related to the decoupling of the stress-transferring rigid nanofiber network upon

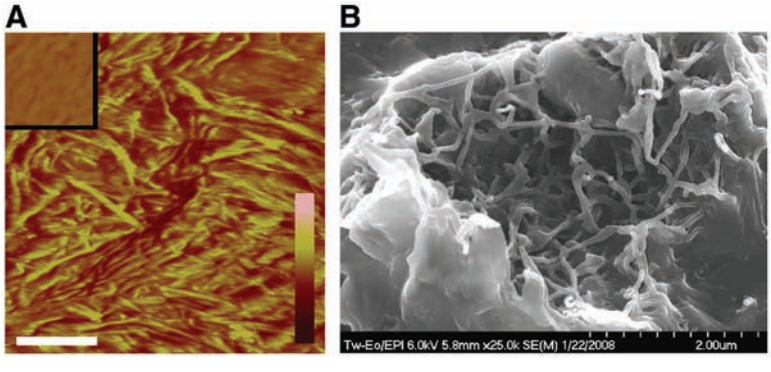

Fig. 3. Morphology of EO-EPI/whisker nanocomposites. (**A**) Representative AFM phase image of an ultramicrotomed nanocomposite containing 9.5% v/v whiskers in EO-EPI. The inset shows an AFM phase image of a neat EO-EPI reference (horizontal scale bar = 500 nm, vertical scale bar = phase shift 120 to 0°). The samples were briefly (10 s) immersed in tetrahydrofuran and rinsed with IPA to partially dissolve the polymer at the surface of the sample and to expose the inner structure of the films. (**B**) Representative SEM image of an untreated nanocomposite containing 9.5% v/v whiskers in EO-EPI.

introduction of water as a competitive hydrogen-bonding agent. Consistent with the proposed mechanism, the switching is fully reversible: The materials adapted their original stiffness upon drying (Fig. 2A).

To investigate the specificity of the switching mechanism, we investigated the effect of isopropanol (IPA) as the swelling agent. IPA was selected because it swells neat EO-EPI to a similar degree as water (Fig. 2B) but is incapable of dispersing cellulose whiskers (*16*). The nanocomposites swelled upon immersion in IPA (Fig. 2B) to a level similar to that of the composites in water; however E' barely changed in comparison to the dry state (Fig. 2C), and the data fit the percolation model. This result confirms that the chemomechanical response is largely a result of disruption of the whisker-whisker interactions and not just plasticization of the material. By contrast, EO-EPI is plasticized considerably upon IPA swelling (E' drops from 3.6 to 0.93 MPa). This contrast highlights the most important advantage of the nanocomposite approach over simple plasticization of a neat polymer. Although plasticization through solvent uptake, which is inherent to the latter, is a nonspecific process, the responsive nanocomposites can be designed to display a response that is specific to the nature of the stimulus. In addition, the nanocomposite approach provides the ability to increase the initial stiffness and strength of the material and allows for the use of host polymers that have no thermal transition in the temperature regime of interest, such as the EO-EPI matrix used here.

We are interested in exploiting dynamic mechanical materials in biomedical applications, specifically as adaptive substrates for intracortical microelectrodes. These implants have the ability to record brain unit activity (*24*). Brain-machine interfaces that rely on these electrodes provide solutions to medical conditions such as Parkinson's disease, stroke, and spinal chord injuries (*25*). One problem with current microelectrodes is that the signal quality usually degrades within a few months, making chronic applications challenging (*26*). One hypothesis for the cause of possible failure, especially in recording applications, is that the micromotion of rigid electrodes within the soft cortical tissue chronically inflicts trauma on the surrounding neurons (*27*). We hypothesize that a mechanically adaptive electrode could alleviate this problem, and we are thus interested in designing devices that are initially rigid to allow for penetration of the pia mater during implantation (*28*) but that soften slowly and without excessive expansion upon implantation in response to the chemical environment within the brain (for an emulation, see Movie S1). For this application, an initial E' of >4 GPa is desirable to allow for the insertion of an electrode with typical dimensions into the cortex (*29*). Because EO-EPI/whisker nanocomposites display a substantially lower E', we sought to combine the switching mechanism with a chemically influenced thermal transition. We discovered that nanocomposites based on poly(vinyl acetate) (PVAc) (Fig. 1C) and cellulose whiskers display such a "dual" responsive behavior. Our data show that, upon exposure to physiological conditions, the materials undergo a phase transition; in addition, the reinforcing whisker network is disassembled. DMA experiments (Fig. 4A and fig. S8) reveal that the neat PVAc displays a T_g around 42°C, that, just above physiological temperature. E'_s of the neat polymer is considerably reduced upon heating from room temperature (1.8 GPa at 23°C) to above T_g (0.39 MPa at 56°C) (this corresponds to T_g + 16°C and marks the temperature at which E'_s is starting to level off). As evidenced by DMA data, the introduction of cellulose whiskers into PVAc has only a minimal influence on T_g in the dry state (Fig. 4A and fig. S8). The thermal transition is sharpened, and the temperature at which E' begins to drop is increased from ~25 to >40°C. For certain biomedical applications, this effect is very desirable, because it prevents the thermally induced softening of the material just upon exposure to body temperature. As a consequence of the already rather high stiffness of the glassy PVAc matrix, only a modest reinforcement is observed for the nanocomposites below T_g (E' = 5.1 GPa with 16.5% v/v whiskers) (fig. S8). However, a dramatic effect is observed above T_g, where E' is increased from 1.0 MPa for the neat polymer matrix up to 814 MPa with 16.5% v/v whiskers (at 56°C). The experimental data above T_g match well with the percolation model (fig. S8), which indicates that also in this series a percolating network of strongly interacting whiskers is formed (*15*, *16*, *18*). The nanocomposites demonstrate significant swelling in both deionized water and artificial cerebrospinal fluid (ACSF). The solvent uptake increases with increasing whisker content and temperature (fig. S9), lowers the T_g to below physiological temperature (19 to 23°C) (fig. S10), and reduces E' dramatically. For example, the E' of a 16.5% v/v whisker nanocomposite above T_g is reduced from 814 MPa (dry) to 10.8 MPa (water swollen; data are for 56 and 37°C, respectively, that is, 16°C above the respective T_g). As for the water-swollen EO-EPI/whisker nanocomposites, the moduli of the ACSF swollen PVAc/whisker nanocomposites are better described by the Halpin-Kardos than the percolation model (fig. S8), again indicative of decoupling of the stress-transferring nanofiber network upon introduction of water.

Exposure to brain tissue, simulated here by immersing the samples into ACSF and heating to

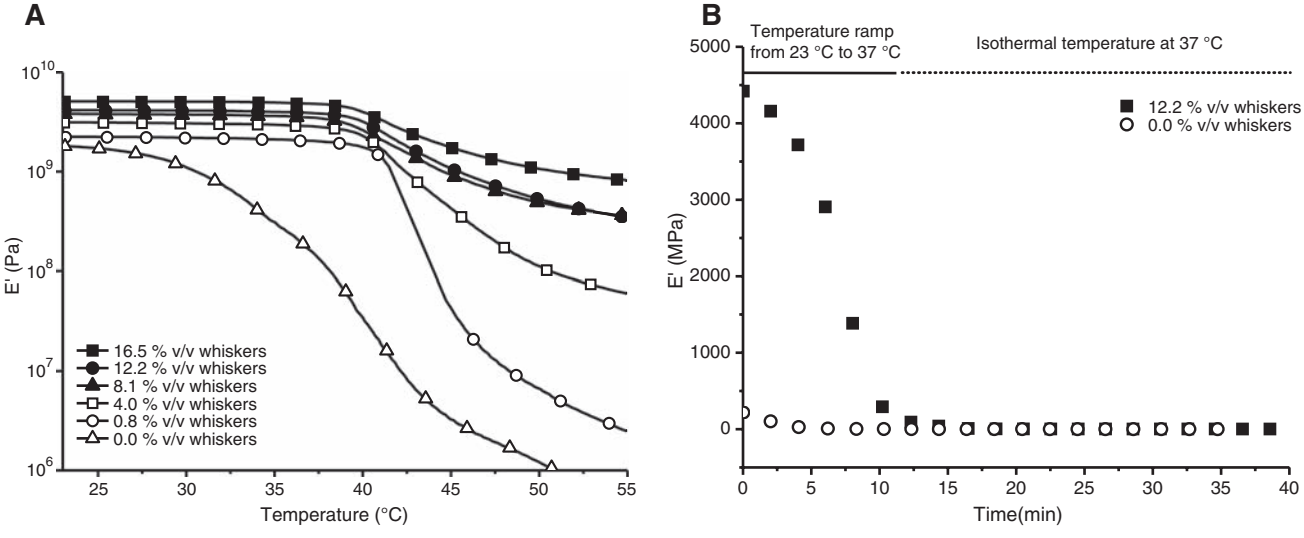

Fig. 4. PVAc/whisker nanocomposites. (**A**) Tensile storage moduli E' of dry films of PVAc/whisker nanocomposites as a function of temperature. The nanocomposites contain between 0 and 16.5% v/v whiskers. (**B**) Time-dependent modulus decrease of neat PVAc and a 12.2% v/v PVAc/whisker nanocomposite upon immersion into ACSF and increasing the temperature from 23°C to 37°C. Lines represent time required for temperature to increase from 23°C to 37°C and isothermal control at 37°C.

a physiological temperature of 37°C at ~2°C/min (*30*) (Movie S1), leads to a pronounced reduction of E'. Whereas the neat PVAc (dry E'_s = 1.8 GPa at 25°C) instantly softens under these conditions (Fig. 4B), the E' of the whisker-reinforced nanocomposites (see Fig. 4B for a 12.2% v/v nanocomposite) is reduced slowly over a period of 15 min. The whisker-reinforced nanocomposite displays a much higher dry E' (4.2 GPa at 25°C) than the neat PVAc, but both materials reach nearly identical moduli upon immersion in ACSF at 37°C (1.6 MPa).

Our data support a simple and versatile strategy for the creation of polymer nanocomposites, whose architecture and mechanical adaptability closely mimic the proposed architecture and observed response of the sea cucumber dermis. The mechanical properties of these chemoresponsive materials can selectively and reversibly be controlled through the formation and decoupling of a three-dimensional network of well-individualized nanofibers in response to specific chemical triggers. It will be interesting to explore whether the framework can be adapted to nonchemical triggers, for example, optical or electrical stimuli.

References and Notes

1. T. Heinzeller, J. Nebelsick, Eds., *Echinoderms* (Taylor & Francis, London, **2004**).
2. T. Motokawa, *Comp. Biochem. Physiol. B* **109**, 613 (1994).
3. F. A. Thurmond, J. A. Trotter, *J. Exp. Biol.* **199**, 1817 (1996).
4. I. C. Wilkie, *J. Exp. Biol.* **205**, 159 (2002).
5. J. A. Trotter, T. J. Koob, *Matrix Biol.* **18**, 569 (1999).
6. G. K. Szulgit, R. E. Shadwick, *J. Exp. Biol.* **203**, 1539 (2000).
7. J. A. Trotter *et al.*, *Biochem. Soc. Trans.* **28**, 357 (2000).
8. J. C. Grunlan, L. Liu, Y. S. Kim, *Nano Lett.* **6**, 911 (2006).
9. M. M. de Souza Lima, R. Borsali, *Macromol. Rapid Commun.* **25**, 771 (2004).
10. J. A. Jaber, J. B. Schlenoff, *J. Am. Chem. Soc.* **128**, 2940 (2006).
11. D. M. Loveless, S. L. Jeon, S. L. Craïg, *J. Mater. Chem.* **17**, 56 (2007).
12. P. S. Belton, S. F. Tanner, N. Cartier, H. Chanzy, *Macromolecules* **22**, 1615 (1989).
13. A. Sturcova, J. R. Davies, S. J. Eichhorn, *Biomacromolecules* **6**, 1055 (2005).
14. O. van den Berg, J. R. Capadona, C. Weder, *Biomacromolecules* **8**, 1353 (2007).
15. M. A. S. Azizi Samir, F. Alloin, A. Dufresne, *Biomacromolecules* **6**, 612 (2005).
16. J. R. Capadona *et al.*, *Nat. Nanotech.* **2**, 765 (2007).
17. M. Takayanagi, S. Uemura, S. Minami, *J. Polym. Sci. C* **5**, 113 (1964).
18. N. Ouali, J. Y. Cavaillé, J. Pérez, *J. Plast. Rubber Comp. Process. Appl.* **16**, 55 (1991).
19. Swelling increased the volume of the nanocomposites and reduced the volume fraction of whiskers, X_r. For example, when a nanocomposite with X_r = 19% v/v was swollen with water, X_r decreased to 14%. The representation of data in Fig. 2A considers this effect to allow for analysis by the Halpin-Kardos model. A direct comparison of dry versus wet composites for the same fiber loading is shown in fig. S6.
20. J. Kunzelman, B. R. Crenshaw, C. Weder, *J. Mater. Chem.* **17**, 2989 (2007).
21. J. C. Halpin, J. L. Kardos, *J. Appl. Phys.* **43**, 2235 (1972).
22. P. Hajji, J. Y. Cavaillé, V. Favier, C. Gauthier, G. Vigier, *Polym. Compos.* **17**, 612 (1996).
23. $\eta_L = [(E_{lr} / E'_s) - 1]/[(E_{lr} / E'_s) + 2A]$, and $\eta_T = [(E_{tr} / E'_s) - 1]/[(E_{tr} / E'_s) + 2]$. A is the aspect ratio of the whiskers, ϕ is equal to the volume fraction of the phase, and the subscripts s and r represent the soft phase and the rigid phase, respectively. E_{lr} is the longitudinal Young's Modulus (130 GPa), and E_{tr} is the transverse Young's Modulus (5 GPa) of an individual cellulose whisker (*22*). To determine the tensile storage modulus of the isotropic nanocomposite (E'), E'_L and E'_T must be inserted into one equation using the Halpin-Kardos model: $E' = 4U_5(U_1 - U_5)/U_1$ where $U_1 = 1/8(3Q_{11} + 3Q_{22} + 4Q_{66})$; $U_5 = 1/8(Q_{11} + Q_{22} - 2Q_{12} + 4Q_{66})$; $Q_{11} = E'_L/(1 - \nu_{12}\nu_{21})$; $Q_{22} = E'_T(1 - \nu_{12}\nu_{21})$; $Q_{12} = \nu_{12}Q_{22} = \nu_{21}Q_{11}$; $Q_{66} = G_{12}$; $\nu_{12} = \phi_r\nu_r + \phi_s\nu_s$ = 0.3; $G_{12} = G_s(1 + \eta\phi_r)/(1 - \eta\phi_r)$; $\eta = (G_r/G_s - 1)/(G_r/G_s + 1)$, ν is the Poisson's ratio, G is the shear modulus, and G_r = 1.77 GPa.
24. D. M. Taylor, S. I. H. Tillery, A. B. Schwartz, *Science* **296**, 1829 (2002).
25. A. B. Schwartz, *Annu. Rev. Neurosci.* **27**, 487 (2004).
26. R. Biran, D. C. Martin, P. A. Tresco, *J. Biomed. Mater. Res.* **82A**, 169 (2007).
27. W. L. C. Rutten, *Annu. Rev. Biomed. Eng.* **4**, 407 (2002).
28. D. H. Szarowski *et al.*, *Brain Res.* **983**, 23 (2003).
29. K. Najafi, J. F. Hetke, *IEEE Trans. Biomed. Eng.* **37**, 474 (1990).
30. Materials and methods are available as supporting material on *Science* Online.

31. We thank F. Carpenter for the photography of the sea cucumber and L. McCorkle, J. Johnson, and M. Hitomi for assistance with the SEM, AFM, and TEM experiments, respectively. Financial support from DuPont (Young Professor Award to C.W.), the L. Stokes Cleveland VAMC Advanced Platform Technology Center, an Ohio Innovation Incentive Fellowship (to K.S.), the Department of Veterans Affairs Associate Investigator Career Development Program (to J.C.), and the National Institutes of Health are gratefully acknowledged. The authors declare that they have no competing financial interest.

Supporting Online Material

www.sciencemag.org/cgi/content/full/319/5868/1370/DC1
Materials and Methods
Figs. S1 to 10
Table S1
References
Movie S1

6 November 2007; accepted 1 February 2008
10.1126/science.1153307

Heterogeneous Nucleation Experiments Bridging the Scale from Molecular Ion Clusters to Nanoparticles

Paul M. Winkler,[1] Gerhard Steiner,[1] Aron Vrtala,[1] Hanna Vehkamäki,[2] Madis Noppel,[3] Kari E. J. Lehtinen,[4] Georg P. Reischl,[1] Paul E. Wagner,[1] Markku Kulmala[2]*

Generation, investigation, and manipulation of nanostructured materials are of fundamental and practical importance for several disciplines, including materials science and medicine. Recently, atmospheric new particle formation in the nanometer-size range has been found to be a global phenomenon. Still, its detailed mechanisms are mostly unknown, largely depending on the incapability to generate and measure nanoparticles in a controlled way. In our experiments, an organic vapor (*n*-propanol) condenses on molecular ions, as well as on charged and uncharged inorganic nanoparticles, via initial activation by heterogeneous nucleation. We found a smooth transition in activation behavior as a function of size and activation to occur well before the onset of homogeneous nucleation. Furthermore, nucleation enhancement for charged particles and a substantial negative sign preference were quantitatively detected.

Condensational growth, evaporation, and heterogeneous chemistry are important phenomena in materials science, fluid dynamics, aerosol physics and technology, and atmospheric chemistry, including cloud microphysics and cloud chemistry. A prerequisite for the start of condensation is homogeneous nucleation of new particles or the activation of preexisting particles by heterogeneous nucleation. The latter can occur either on ions, soluble particles, or insoluble particles, and is energetically easier than homogeneous nucleation (*1*). Both particle formation processes are of fundamental as well as practical importance and have been the subject of investigations for more than a century (*2*). Important examples representing the different processes are given by the use of the Wilson cloud chamber (*3*) in high-energy physics for the case of ions, the formation of cloud droplets in the troposphere for the case of soluble particles, and the occurrence of ice nucleation for the case of insoluble seed particles (*4*). Atmospheric observations suggest that the initial formation and growth are two uncoupled processes (*5*–*7*), and therefore the activation mechanism of small clusters is of vital importance. Understanding the formation and initial growth processes in detail is also crucial to control the production of nanomaterials (*8*).

In this paper, we present experimental results for the activation of molecular cluster ions, charged and neutral clusters, and nanometer-size particles having almost monodisperse size distributions,

[1]Fakultät für Physik, Universität Wien, Boltzmanngasse 5, A-1090 Wien, Austria. [2]University of Helsinki, Department of Physical Sciences, Post Office Box 64, 00014 University of Helsinki, Finland. [3]Institute of Physics, University of Tartu, 18 Ülikooli Street, 50090 Tartu, Estonia. [4]Department of Physics, University of Kuopio and Finnish Meteorological Institute, Post Office Box 1627, 70211 Kuopio, Finland.

*To whom correspondence should be addressed. E-mail: markku.kulmala@helsinki.fi